Biogeosciences, 11, 75–90, 2014
www.biogeosciences.net/11/75/2014/
doi:10.5194/bg-11-75-2014

Biogeosciences Open Access

Observed small spatial scale and seasonal variability of the CO_2 system in the Southern Ocean

L. Resplandy[1,*], **J. Boutin**[1], **and L. Merlivat**[1]

[1]LOCEAN (CNRS, IRD, MNHN, UPMC), UMR 7159, Paris, France
[*]now at: Laboratoire des sciences du climat et de l'environnement (LSCE) – UMR8212, Gif sur Yvette, France

Correspondence to: L. Resplandy (laure.resplandy@lsce.ipsl.fr)

Received: 19 June 2013 – Published in Biogeosciences Discuss.: 22 August 2013
Revised: 14 November 2013 – Accepted: 18 November 2013 – Published: 7 January 2014

Abstract. The considerable uncertainties in the carbon budget of the Southern Ocean are largely attributed to unresolved variability, in particular at a seasonal timescale and small spatial scale ($\sim$ 100 km). In this study, the variability of surface pCO_2 and dissolved inorganic carbon (DIC) at seasonal and small spatial scales is examined using a data set of surface drifters including $\sim$ 80 000 measurements at high spatiotemporal resolution. On spatial scales of 100 km, we find gradients ranging from 5 to 50 µatm for pCO_2 and 2 to 30 µmol kg^{-1} for DIC, with highest values in energetic and frontal regions. This result is supported by a second estimate obtained with sea surface temperature (SST) satellite images and local DIC–SST relationships derived from drifter observations. We find that dynamical processes drive the variability of DIC at small spatial scale in most regions of the Southern Ocean and the cascade of large-scale gradients down to small spatial scales, leading to gradients up to 15 µmol kg^{-1} over 100 km. Although the role of biological activity is more localized, it enhances the variability up to 30 µmol kg^{-1} over 100 km. The seasonal cycle of surface DIC is reconstructed following Mahadevan et al. (2011), using an annual climatology of DIC and a monthly climatology of mixed layer depth. This method is evaluated using drifter observations and proves to be a reasonable first-order estimate of the seasonality in the Southern Ocean that could be used to validate model simulations. We find that small spatial-scale structures are a non-negligible source of variability for DIC, with amplitudes of about a third of the variations associated with the seasonality and up to 10 times the magnitude of large-scale gradients. The amplitude of small-scale variability reported here should be kept in mind when inferring temporal changes (seasonality, interannual variability, decadal trends) of the carbon budget from low-resolution observations and models.

1 Introduction

The Southern Ocean is a key region for the global carbon cycle and the climate system. It accounts for about 25–30 % of the total anthropogenic carbon uptake, although its spatial extension differs in the literature (Orr et al., 2001; Mikaloff Fletcher et al., 2006; Gruber et al., 2009; Takahashi et al., 2009). The carbon flux in this region is governed by the balance between a large uptake of anthropogenic CO_2 and a substantial outgassing of natural CO_2 (Lovenduski et al., 2008; Gruber et al., 2009). Despite its importance, the Southern Ocean remains the region where uncertainties regarding the air–sea CO_2 flux and the carbon budget are the highest (e.g., Gruber et al., 2009). Quantifying this subtle balance and its sensitivity to dynamical and biological changes is therefore one of the most challenging issues in assessing today's global carbon budget.

The recent syntheses of Gruber et al. (2009) and Lenton et al. (2013) compared the CO_2 uptake by the Southern Ocean estimated from various models (ocean biogeochemical models, inverse atmospheric and oceanic models) with those derived from observations. Although the mean of all models agree surprisingly well with observations to an uptake of $\sim 0.34 \pm 0.2$ PgC yr^{-1} in both Gruber et al. (2009) and Lenton et al. (2013), individual model results are spread over a wide range, between 0.15 and 0.72 PgC yr^{-1} in Gruber et al. (2009) and between -0.3 (i.e., out-gazing) and 0.3 PgC yr^{-1} in Lenton et al. (2013).

These large discrepancies in the flux are also found between the various estimates derived from observations at the regional level and on seasonal timescales. For example, Barbero et al. (2011) recomputed the CO_2 ocean uptake in the Southern Ocean's Pacific sector using pCO_2 maps extrapolated from observations by McNeil et al. (2007); Boutin et al. (2008); Takahashi et al. (2009); Barbero et al. (2011). From these four methods, the oceanic CO_2 uptake varies between 0.05 and 0.50 PgC yr^{-1}, with highest discrepancies (up to 0.8 PgC yr^{-1}) during winter.

These large uncertainties are primarily attributed to unresolved spatiotemporal variability and to high wind speeds that translate moderate errors in pCO_2 into large errors in air–sea CO_2 fluxes. In this paper, we focus on the issue of unresolved variability. The Southern Ocean is remote and hardly accessible in winter, leading to a very sparse spatiotemporal coverage of hydrographic observations, including measurements of surface pCO_2 (Takahashi et al., 2009; Pfeil et al., 2012). Undersampling biases are aggravated by the high variability this oceanic region displays over a wide range of temporal and spatial scales. A combination of various observation- and model-based methods has recently enabled a better quantification of the air–sea CO_2 flux in the Southern Ocean and its variability at a large spatial scale (e.g Gruber et al., 2009) and interannual timescale (e.g., Séférian et al., 2013). Substantial variability was captured at decadal timescales, with estimates derived from observations and models of the order of 0.05 to 0.15 PgC yr^{-1} (Metzl, 2009; Séférian et al., 2013; Brix et al., 2013) and attributed to sea–ice interactions leading to deep mixing events (Séférian et al., 2013) and the Southern Annular Mode (Brix et al., 2013; Séférian et al., 2013).

The variability introduced at smaller spatial and shorter temporal scales remains largely unknown. Periodic surveys in the Indian sector and a 10 yr time series located south of New Zealand have revealed relatively large variations of oceanic surface pCO_2 at a seasonal timescale (10–40 µatm, Metzl et al., 2006; Brix et al., 2013). Although these surveys provide very useful information, the seasonality of the CO_2 system is still poorly constrained at the basin scale, complicating the interpretation of observations and the evaluation of ocean models in this region. Furthermore, the Southern Ocean is one of the most energetic regions of the world ocean, with numerous mesoscale eddies modulating the dynamical transport of biogeochemical tracers including carbon (Rintoul et al., 2001; Ito et al., 2004; Tortell et al., 2011) and the biological activity (Read et al., 2007; Tortell et al., 2011). The few observations of these small spatial scales are, however, too sparse to assess the role of small-scale structures in the carbon budget.

In this study, we estimate the variability of the CO_2 system introduced by small spatial-scale structures ($\sim$ 100 km) and the seasonality in the Southern Ocean. We combine an extensive data set of surface drifters including $\sim$ 80 000 year-round measurements at high spatiotemporal resolution with satellite and in situ gridded products to quantify the small-scale variability of pCO_2 and dissolved inorganic carbon (DIC), identify the source of this variability (dynamical and/or biological) and compare it to the variability introduced by regional contrasts and the seasonality. Section 2 describes the observations and the various methods used. Section 3 examines the variability of surface pCO_2 and DIC in a case study of the area around Crozet Island before extending the analysis to the Southern Ocean. Finally, Sect. 4 synthesizes and discusses the main results.

2 Methods

2.1 Observations

2.1.1 CARIOCA drifters

Between 2003 and 2009, nine autonomous Lagrangian CARbon Interface OCean Atmosphere (CARIOCA) drifters were deployed in the Southern Ocean, acquiring an extensive data set of 80 537 individual observations. The region covered by our observations extends from south of the polar front (55° S) to north of the subtropical front (40° S), with most observations acquired in the subantarctic and subtropical zone of the Southern Ocean (Fig. 1a). CARIOCA drifters hourly measure CO_2 fugacity (fCO_2), sea surface temperature (SST), sea surface salinity (SSS) and fluorescence at a depth of 2 m (Copin-Montégut et al., 2004; Boutin et al., 2008). Extensive validation of CARIOCA measurements in the Southern Ocean indicate an absolute (relative) precision close to 3 (1) microatm (see Appendix of Boutin et al., 2008). Alkalinity is derived from SSS and SST using a formulation by Lee et al. (2006); DIC is derived from fCO_2, alkalinity, SST and SSS using CO_2 dissociation constants and solubility as described in Boutin et al. (2008). The unit for DIC is µmol kg^{-1}. The relative precision of successive DIC values is expected to be 0.5 µmol kg^{-1}. In order to avoid artificial diurnal cycle of fluorescence created by the quenching effect, we consider daily average fluorescence. Finally, to allow comparison, float observations and the Glodap (Global Ocean Data Analysis Project) climatology were normalized to the year 2005, assuming linear drifts of 0.7 µmol kg^{-1} yr^{-1} for DIC and 1.4 µatm yr^{-1} for pCO_2 (Takahashi et al., 2009; Boutin and Merlivat, 2009).

2.1.2 Satellite data and global climatologies

We use 3-D-gridded DIC fields from Glodap (Key et al., 2004, ;data available online at: cdiac.ornl.gov/ftp/oceans/GLODAP) and Satellite SSTs from Advanced Microwave Scanning Radiometer-Earth Observing System (AMSR-E, www.ghcc.msfc.nasa.gov/AMSR/), both collocated in time and space with drifter measurements using nearest-neighbor interpolation. Fronts and transport barriers delimiting small-scale structures are computed in the subantarctic frontal

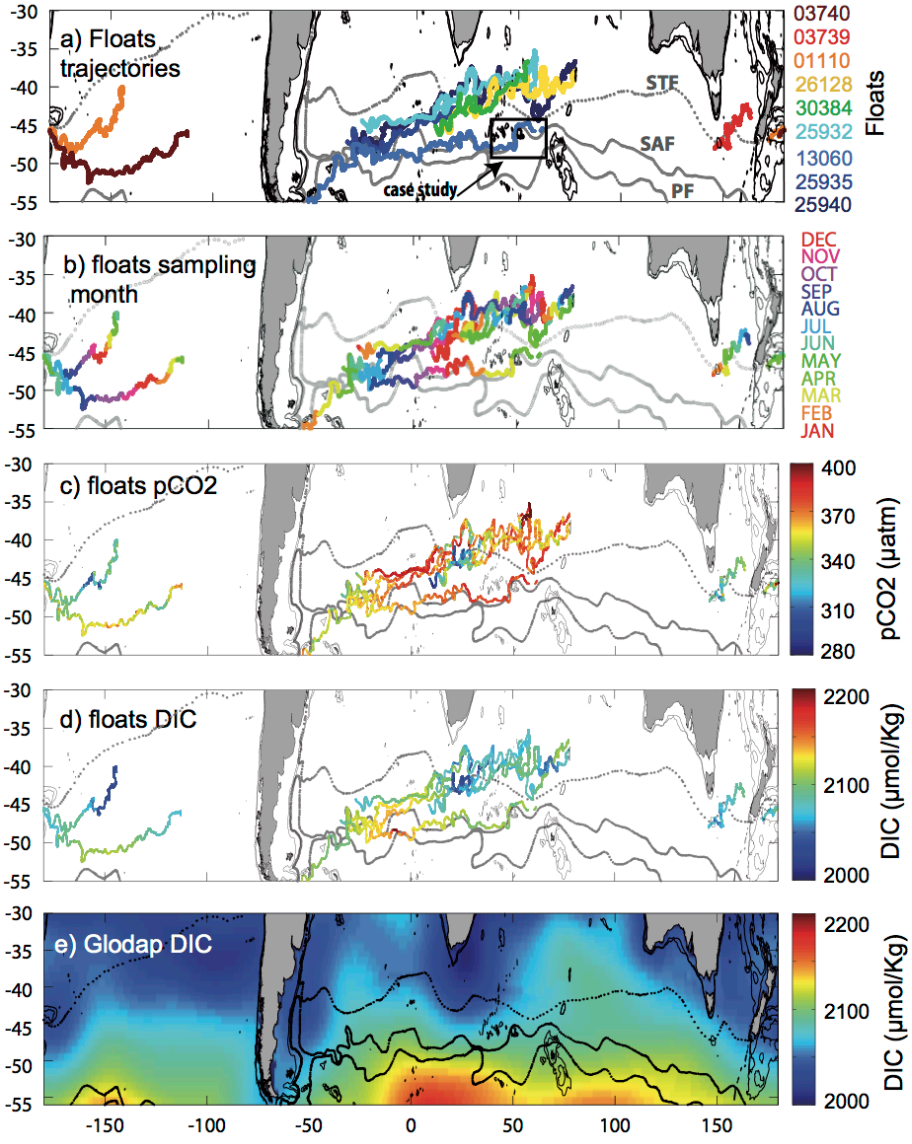

Fig. 1. (a) Drifters trajectories; **(b)** drifters sampling month; **(c)** drifters pCO_2 (in µatm); **(d)** drifters DIC (in µmol kg^{-1}) and **(e)** DIC in Glodap database (in µmol kg^{-1}). A correction of 0.7 µmol kg^{-1} yr^{-1} has been applied to reference all DIC observations to the year 2005.

zone around the Crozet Plateau. This is performed using Lagrangian coherent structures embedded in the velocity field with finite-size Lyapunov exponent technique (d'Ovidio et al., 2004; Lehahn et al., 2007). Velocity fields are from a Ssalto/Duacs Aviso altimetry product (available online at www.aviso.oceanobs.com/en/data/product-information/duacs/).

2.2 Assessing small-scale variability SV100km diagnostic

We quantified the variability of pCO_2 and DIC at small scales using the nine drifters' extensive data set. CARIOCA drifters sample with a horizontal resolution of 1 to 3 km (drifting speed of $\sim$0.3–0.9 m s^{-1} and hourly sampling), hence distinctly capturing the variability at the mesoscale ($\sim$ 100 km). The contribution of the mesoscale was disentangled from the large-scale and seasonal signal also captured by the drifters using a fast Fourier transform 20-day high-pass filter. This allowed us to filter out variations with timescales larger than 20 days (seasonal signal) and with spatial scales larger than $\sim$ 500–1000 km (distance covered with a drifting speed of $\sim$ 0.3–0.9 m s^{-1} in 20 days). In the following, $\widehat{X}$ denotes the anomaly of the field X associated with small scales obtained with the high-pass filter. The spatial variability of pCO_2 and DIC at small spatial scale is then evaluated using the diagnostic SV100km that quantifies the

spatial variability on scales of 100 km (see Sect. 3.1.2). At each point, t, of the trajectory, SV100km is defined as the amplitude of variation (maximum sampled value − minimum sampled value) in a 100 km × 100 km box centered on the point:

$$\mathrm{SV100km}(t) = \max(\widehat{X}(t, 100\,\mathrm{km})) - \min(\widehat{X}(t, 100\,\mathrm{km})), \quad (1)$$

where $\widehat{X}(t, 100\,\mathrm{km})$ is the time series of the high-pass filtered field X included in a box of 100 km × 100 km centered on t.

SV100km was also evaluated using a second method combining drifters measurements and satellite observations (see Sect. 3.3). This method relies on the frequent linear correlation found locally between $\widehat{\mathrm{DIC}}$ and $\widehat{\mathrm{SST}}$ on small spatial scales. The existence of a "local" relationship between a carbon variable (namely $p\mathrm{CO_2}$) and SST was identified by Chen et al. (2007) across one eddy in the tropical Pacific. Here, we derive such local linear correlations between $\widehat{\mathrm{DIC}}$ and $\widehat{\mathrm{SST}}$ using 20-day sliding windows covering the complete data set (Eq. 2.2). Two-dimensional maps of DIC anomaly (noted $\widehat{\mathrm{DIC}}_{\mathrm{sat}}$) were then reconstructed by applying the local linear relationship obtained from in situ observations to $\widehat{\mathrm{SST}}_{\mathrm{sat}}$ derived from AMSR-E satellite observations in 100 km × 100 km boxes around the float location (Eq. 2.2). Here, $\widehat{\mathrm{SST}}_{\mathrm{sat}}$ is the SST anomaly obtained by removing the mean SST in each 100 km × 100 km box. The reconstruction was performed only for correlation coefficients $r^2 \geq 0.7$ (see Fig. 8). Here, $\mathrm{SV100km}_{\mathrm{sat}}$ is computed from a 2-D spatial map of DIC anomaly at a given time in a 100 km × 100 km box around the point i (Eq. 2.2), whereas in the first method, SV100km is computed from the time series of DIC included in the same 100 km × 100 km box (Eq. 2).

$$\widehat{\mathrm{DIC}} = a \cdot \widehat{\mathrm{SST}} + b, \quad (2)$$

$$\widehat{\mathrm{DIC}}_{\mathrm{sat}} = a \cdot \widehat{\mathrm{SST}}_{\mathrm{sat}} + b \quad (3)$$

$$\mathrm{SV100km}_{\mathrm{sat}}(i) = \max(\widehat{X}(i, 100\,\mathrm{km}_{\mathrm{sat}})) - \min(\widehat{X}(i, 100\,\mathrm{km}_{\mathrm{sat}})) \quad (4)$$

,

where $\widehat{X}(i, 100\,\mathrm{km})$ is the map of $\widehat{X}$ included in a box of 100 km × 100 km centered on i.

2.3 Drivers of small-scale variability Principal Component Analysis

The mechanisms driving the variability at a small scale quantified by SV100km are examined using principal component analysis (PCA). PCA, also known as empirical orthogonal function analysis, has been widely used to explore the major factors that give rise to variability patterns in geosciences and in particular to surface $p\mathrm{CO_2}$ variability (Dandonneau, 1995; Murata, 2006; Lohrenz et al., 2009). Here, we use this technique to examine how the variability at small spatial scales in the $\mathrm{CO_2}$ system, and more specifically in DIC concentrations, relates to the variability of SST and fluorescence, a signature of biological processes. The choice of DIC over $p\mathrm{CO_2}$ for this analysis was made with the aim of disentangling the contribution of dynamical processes that influences $p\mathrm{CO_2}$ through DIC and SST from the thermodynamical effect that only affects $p\mathrm{CO_2}$. Furthermore, model- and observation-based studies concur with the fact that DIC is the main driver of surface $p\mathrm{CO_2}$ variability in the Southern Ocean (Metzl et al., 2006; Lovenduski et al., 2008; Metzl, 2009; Brix et al., 2013; Séférian et al., 2013). Surface DIC concentrations generally vary with physical and/or biological factors, such as vertical and lateral dynamical transport or biological uptake by photosynthesis. However, the objective here is not to directly explain variations of DIC by variations in SST and fluorescence (Fluo) but to relate the small-scale spatial variability in DIC to either dynamical or biological factors and identify where and when those variations are dominant. The PCA is a useful tool in that context, as it correlates the relative variations of DIC with the relative variations of SST and fluorescence after having centered and normalized the variables relative to their mean and standard deviation, respectively. The factors driving the variability of DIC at small scales are likely to be different depending on the region and time of year. We therefore chose not to compute one PCA with the complete CARIOCA data set. Instead, we compute "local PCAs" over segments of the drifters' trajectory to identify the factors driving the variability at small spatial scales. This approach differs from those of Dandonneau (1995); Murata (2006) and Lohrenz et al. (2009), in which one PCA was computed with the complete data set and for relatively smaller regions.

As in the method used to assess small-scale variability, PCAs are performed on $\widehat{\mathrm{Fluo}}$, $\widehat{\mathrm{SST}}$ and $\widehat{\mathrm{DIC}}$ (i.e., filtered from variations with scales > 20 days and > 500–1000 km, see Sect. 2.2) and normalized to an average of 0 and a standard deviation of 1 (noted $\widehat{\mathrm{Fluo}}_n$, $\widehat{\mathrm{SST}}_n$ and $\widehat{\mathrm{DIC}}_n$). At each point of the drifters trajectory, a PCA is computed over a 20-day window centered on the point with a data set of 480 rows (hourly measurements over 20 days) and 3 columns ($\widehat{\mathrm{Fluo}}_n$, $\widehat{\mathrm{SST}}_n$ and $\widehat{\mathrm{DIC}}_n$). Each of the ∼ 80 000 PCAs gives 3 "local principal components" (noted PC1, PC2 and PC3) and the variance explained by each of the PCs. For example, at 11.3° W/–45.3° N the PCA gives the following result:

$$\mathrm{PC1} = 0.63083 \cdot \widehat{\mathrm{SST}}_n + 0.46049 \cdot \widehat{\mathrm{Fluo}}_n - 0.62450 \cdot \widehat{\mathrm{DIC}}_n,$$

$$\mathrm{PC2} = 0.30271 \cdot \widehat{\mathrm{SST}}_n - 0.88713 \cdot \widehat{\mathrm{Fluo}}_n - 0.34838 \cdot \widehat{\mathrm{DIC}}_n,$$

$$\mathrm{PC3} = 0.460492 \cdot \widehat{\mathrm{SST}}_n - 0.887132 \cdot \widehat{\mathrm{Fluo}}_n + 0.030727 \cdot \widehat{\mathrm{DIC}}_n,$$

with PC1, PC2 and PC3, respectively, explaining 73 %, 22 % and 5 % of the variance.

The contribution of the normalized variables to the PC is given by their loading (for example −0.6245 for DIC_n on PC1), its sign having the same meaning as the sign of a correlation coefficient. In this example, most of the variability

is explained by PC1 (73 %) and is characterized by opposed variations of SST and DIC. In the following, only PC1 and PC2 that significantly contribute to DIC small-scale variability (i.e., with explained variance greater than 20 % and cumulative contribution exceeding 80 %) are considered (see Sects. 3.1.1 and 3.2.2). Note that PCAs were not performed along the drifter 01110, for which fluorescence was not available (Fig. 1a).

3 Results

The variability of the CO_2 system at small spatial scale (i.e., ~ 100 km) and the processes driving this variability are first presented in a case study region around the Crozet Plateau. Then, the results are extended to the Southern Ocean using the observations of the nine drifters.

3.1 Observed variability of the CO_2 system at a small scale

3.1.1 Case study – subantarctic frontal zone and Crozet Plateau

-5mm The case study is focused on a drifter drifting in the southwest Indian Ocean, more specifically in the subantarctic frontal zone and across the Crozet Plateau (20–60° E, 50–42° S), between December 2006 and April 2007 (Fig. 1a). The drifter followed a path characteristic of surface drifters in this area (Pollard et al., 2007). After drifting along the Subantarctic Front (SAF), it crossed the Southwest Indian Ridge in January 2007, where the Polar Front (PF) and SAF combine in what is the major pathway of the Antarctic Circumpolar Current (ACC) across the ridge (35° E–48° S, Fig. 2). After following the SAF, the drifter headed north along the Subantarctic Front between the Del Caño Rise and Crozet in March ($\sim 48°$ E) and then drifted east through the Crozet Plateau in late April (Fig. 2). The evolution of pCO_2, DIC, SST and Fluo along this trajectory are modulated by the presence of the SAF, separating cold/DIC-rich southern waters from warmer/DIC-poor northern waters, and the presence of the Crozet Plateau, known to be biologically active with a bloom occurring annually between September and January (Venables et al., 2007). For example, high surface pCO_2 (up to 388 µatm) is maintained west of the ridge by either high DIC/low SST southern waters or relatively high SST/low DIC northern waters (Fig. 2a, c and g). By contrast, low pCO_2 sampled north of Crozet is associated with low DIC/high Fluo waters (Fig. 2a, c, e and g).

The variability at small spatial scales is highlighted by filtering out scales > 20 days and > 500–1000 km (see Sect. 3.1.2). The resulting anomalies in pCO_2, DIC, SST and fluorescence fields highlight the hotspots of variability at small spatial scales (Fig. 2 right-hand panels). Although the position of the fronts indicated here is climatological and not collocated in time with the position of the drifter, most hotspots of variability are located in the vicinity of the front. This is not surprising as density fronts are a major generator of mesoscale eddies and potential dynamical and biological boundaries with contrasting properties on either side. The strength of the CO_2 system variability at small spatial scales is estimated using the diagnostic SV100km that quantifies the variability in 100 km $\times$ 100 km boxes (see Sect. 3.1.2 for details). Highest SV100km are found north of Crozet, with small-scale variations of $pCO_2 \geq 15$ µatm and small-scale variations of DIC ≥ 12 µmol kg^{-1} (Fig. 2i, j). By contrast, areas of lowest variability are found south of Del Caño Rise, where SV100km is of the order of 5 µatm and 3 µmol kg^{-1} for pCO_2 and DIC respectively (Fig. 2i, j).

3.1.2 A first estimate for the Southern Ocean

The variability of pCO_2 and DIC at a small spatial scale is estimated using the diagnostic SV100km computed along the nine drifters' trajectories (Fig. 3a, b). Although the drifter in the case study crossed the SAF and the Crozet Plateau, the variability identified in this area is relatively low compared to other regions of the Southern Ocean. Highest variability of the CO_2 system is found in the energetic region of the Agulhas, where pCO_2 and DIC horizontal gradients respectively reach values ≥ 20 (up to 50) µatm and ≥ 10 (up to 30) µmol kg^{-1} on spatial scales of 100 km (Fig. 3a, b). Drifters also captured relatively high variability at a small spatial scale close to frontal zones (PF, Subtropical Front (STF) and SAF), where SV100km is of the order of 15–20 µatm and 10–15 µmol kg^{-1} for pCO_2 and DIC respectively. High variability is found in regions of lower eddy kinetic energy (EKE) in the southern Pacific (150° W, 40–45° S and 120° W, 45–50° S). However, when the two drifters 03740 and 01110 sampled this area in 2004, the SAF was located north of its climatological position, which probably explains the high variability captured in this region by the drifters (Barbero et al., 2011). Elsewhere, the variability typically ranges between 5 and 15 µatm and 2 and 10 µmol kg^{-1}.

3.2 Drivers of DIC variability at a small scale

Here we examine how the variability of surface DIC at small spatial scales relates to dynamical processes and biological activity. The respective role of dynamics and biology is identified by correlating observed variations of SST and fluorescence to variations of DIC surface concentrations, using locally derived principal component analyses (PCAs, see Sect. 2.3). The analysis of the PCAs along eight of the

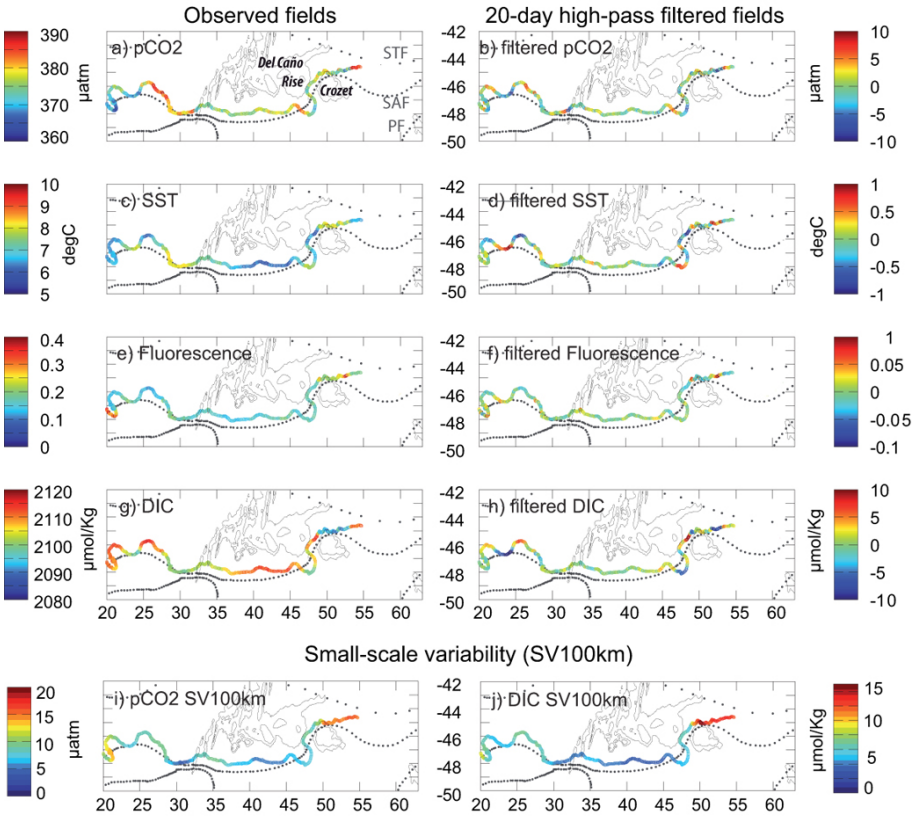

Fig. 2. Case study: drifter 13 060 in the Crozet Plateau area. **(a, c, e, g)** surface pCO_2, SST, fluorescence and DIC; **(b, d, f, h)** 20-day high-pass filtered surface pCO_2, SST, fluorescence and DIC; **(i–j)** SV100km quantifying small-scale spatial variability of pCO_2 and DIC.

drifters reveals three major cases: the variability of DIC at a small scale is either dominated by (1) ocean dynamical processes, (2) biological uptake of DIC or (3) a combination of dynamical and biological processes. Note that we neglect the influence of air–sea fluxes by less than 15 %. We discriminate between the three cases using the loadings of the PCs that are strongly correlated to DIC (i.e., with $|\mathrm{DIC}_n \mathrm{loading}| > 0.3$). In the dynamics-dominated case (denoted DYN), the variability at a small scale is dominated by the signature of anticorrelated large-scale gradients (vertical and/or lateral) of DIC and SST. Indeed, increasing depth and increasing latitude are characterized by decreasing temperature and increasing DIC (Fig. 1e). This case is hence identified by anticorrelated loadings on DIC and SST and a low loading of fluorescence compared to SST ($|\mathrm{SST}_n$ loading$| > |$ Fluo$_n$ loading$| + 0.3$). The biology-dominated case (noted BIO) is identified by anticorrelated loadings on DIC and fluorescence (DIC uptake by biological activity) and low loadings on SST compared to fluorescence (i.e., $|\mathrm{SST}_n$ loading$| < |\mathrm{Fluo}_n$ loading$| + 0.3$). Finally, the dynamics–biology combined case (noted DYN + BIO) correspond to anticorrelated SST and DIC, anticorrelated fluorescence and DIC and similar loadings on SST and fluorescence (i.e., $|\mathrm{SST}_n$ loading$| - |\mathrm{Fluo}_n$ loading$| \leq 0.3$).

3.2.1 Case study – subantarctic frontal zone and Crozet Plateau

The PCA reveals that the majority of the variance at small spatial scales in the case study area is explained by the first and second principal components (PC1 and PC2). Of the total variance, $\sim$ 50 to 70 % is accounted for by PC1, and 20 to 30 % by PC2, leading to a cumulated variance $\geq$ 80 % (Fig. 4a and b). The contribution of PC3 is significantly lower, with a maximum explained variance of 20 % at $\sim 33°$ E (not shown). The fact that PC3 explains a non-negligible part of the variance highlights the fact that SST and fluorescence do not sufficiently explain all variations of the DIC concentration at small spatial scales. However, the objective here is not to directly explain variations of DIC by variations in SST and fluorescence, but to identify if the variability at a small scale can be correlated to either ocean dynamics or biological uptake of DIC. In this region, only PC1 is strongly related to the variations of DIC ($|\mathrm{loadings\ DIC}_n| \leq 0.7$, Fig. 4c). By contrast, DIC contribution to PC2 is weak ($|\mathrm{loadings\ DIC}_n| \leq 0.3$), indicating that PC2 primarily reflects the joint variations of SST and fluorescence (Fig. 4d, f and h). In the following we therefore focus

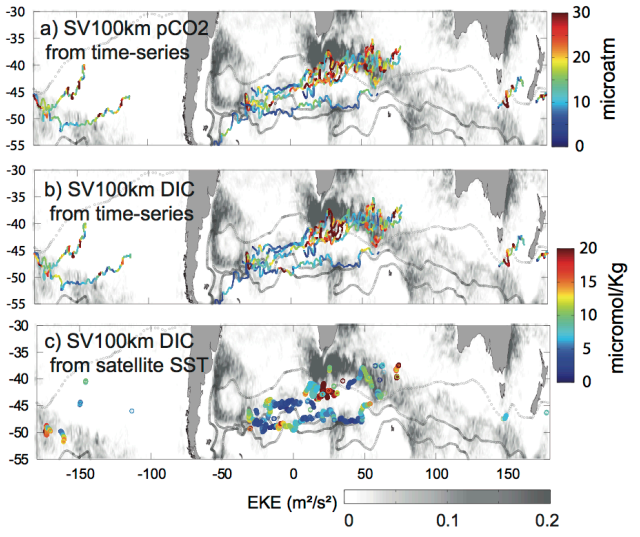

Fig. 3. Eddy kinetic energy (EKE, grey scale) estimated from satellite altimetry and mesoscale variability **(a)** SV100km of in situ pCO_2 (in µatm) and **(b)** SV100km of in situ DIC (in µmol kg^{-1}) estimated from the standard deviation of high-pass filtered fields in 100 km × 100 km boxes along drifters trajectories (see Sect. 3.1.2 for further details), **(c)** SV100km$_{sat}$ of DIC (in µmol kg^{-1}) reconstructed from satellite SST and the local linear correlations between SST and DIC deduced from drifters data. DIC was reconstructed only for correlation coefficients $r^2 > 0$. (Fig. 8), hence explaining the lower spatial coverage of panel **(c)** compared to panel **(b)**. EKE was estimated in 2006 from satellite altimetry as $(u-\overline{u})^2+(v-\overline{v})^2$, where u and v are the zonal and meridional surface current velocities and the overbear denotes the annual mean.

on PC1 that explains most of the DIC variability at small spatial scale.

In this region, PC1 opposes SST and DIC; i.e., a decrease in DIC is correlated to an increase in SST (Fig. 4c and e). This negative correlation is consistent with the opposed large-scale horizontal and vertical gradients of SST and DIC: SST decreases while DIC increases with increasing latitude and depth. In addition, fluorescence is strongly anticorrelated with DIC, in particular on the Crozet Plateau, where the SV100km of pCO_2 and DIC are high (Fig. 4c and g and Fig. 2j). Positive anomalies of fluorescence are associated with positive anomalies of SST, indicating that biological activity is higher north of the SAF (Fig. 2f and h). The dominant drivers of DIC variability are identified using criteria on DIC, SST and fluorescence contribution to PC1 (see details in Sect. 2.3). We find that the ocean dynamics is the major factor explaining the observed variability of DIC at small spatial scale (DYN on Fig. 4i and combines with biological activity north of Crozet (DYN+BIO on Fig. 4i and Fig. 2j). This suggests that the impact of biological activity is more localized than the impact of ocean circulation but plays a crucial role by enhancing the amplitude of DIC variability at small spatial scales.

3.2.2 Southern Ocean

Similarly to the case study, the PCA of DIC, SST and fluorescence reveals that most of the variability is explained by PC1 and PC2; PC1 accounts for 50 to 80 % of the variance (Fig. 5a) and PC2 for 10 to 50 % (Fig. 5b), leading to a cumulated variance explained by PC1 and PC2 $\geq$ 80 % in more than 85 % of the points (Fig. 5c). The contribution of PC3 is significantly lower, with an explained variance $\leq$ 20 % in more than 75 % of the points. For clarity, we show here the processes driving the DIC distribution at small spatial scales identified from PCAs loadings, while the details of PC1, PC2 and PC3 loadings are shown in Appendix A (Figs. 12–A2).

From PC1, ocean dynamics is identified as the major mechanism setting DIC patterns at small scale, in particular between the Polar Front and the Subtropical Front (DYN on Fig. 6a). In these regions, PC1 primarily reflects the large-scale gradients opposing variations of DIC and SST (Fig. 12). By contrast, biological activity emerges as the dominant driver in the region of the Agulhas retroflection (BIO in Fig. 6a). Areas where biological activity dominates are characterized by positive contributions of fluorescence and negative contributions of SST and DIC (Fig. 12). The correlated variations of SST and DIC in these regions contrast with the anti-correlation observed everywhere else (Figs. 12a, b and 6).This suggests that, in these regions, DIC of cold and carbon-rich southern waters has been consumed by biological activity, therefore inverting the signature of the large-scale opposed gradients of DIC and SST. As expected, the contribution of biological activity is higher during summer (Fig 7). However, it should be noted that biological production is also identified as a dominant process for a large number of observations during fall, winter and spring (Fig 7). The major reason is that seasonal variations of DIC, and hence the variations associated with the seasonal bloom, have been filtered out from this analysis. What is highlighted here is the role of biological activity in introducing variability on scales of 100 km.

Finally, in many regions, a combination of both biological activity and ocean circulation influences the DIC distribution at small spatial scales (DYN + BIO on Fig. 6a). In these regions, fluorescence and SST contributions to PC1 are large and negatively correlated to DIC. This suggests that ocean dynamics maintains opposed large-scale gradients of DIC and SST down to small spatial scales, while biological activity could play a significant role in the observed variability at a small scale (Fig. 12). The co-dominance of both factors is identified mainly along frontal areas or in regions of high EKE (Fig. 3). In one of these regions located between 142° W and 134° W in the Pacific sector, the joint contributions of biological activity and ocean circulation identified with the PCA is strongly supported by the work of Barbero et al. (2011). In their work, Barbero et al. (2011) combined satellite chlorophyll a concentrations and net community primary production inferred from diel cycles of in situ DIC

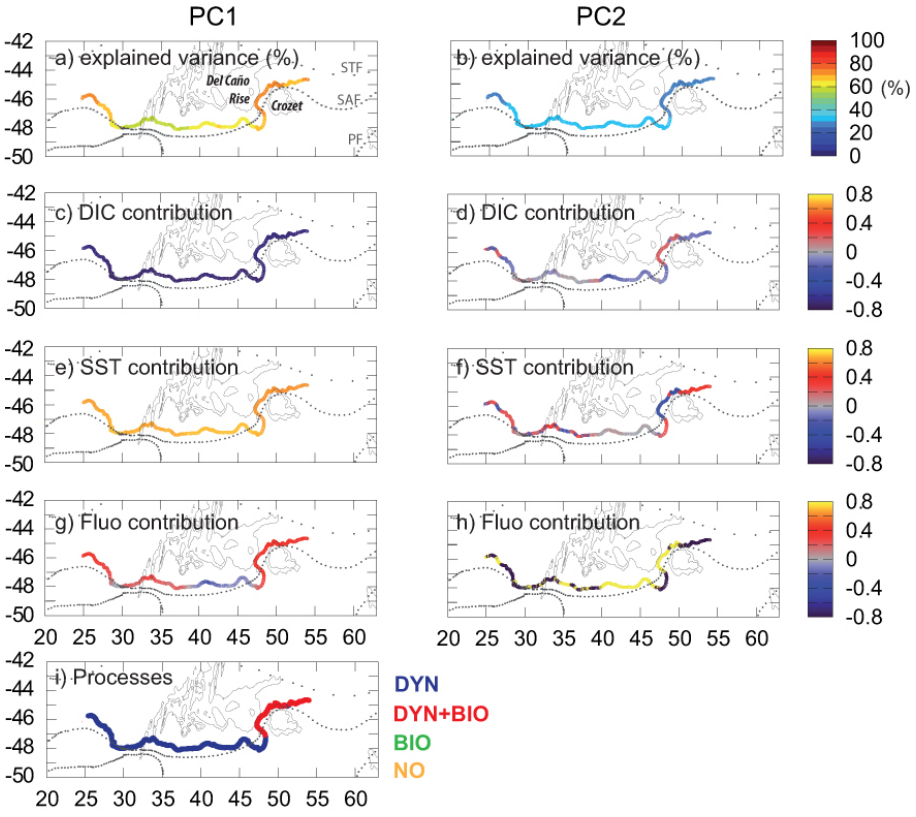

Fig. 4. Principal component analysis in the case study area: explained variance by **(a)** PC1 and **(b)** PC2; DIC loadings for **(c)** PC1 and **(d)** PC2; SST loadings for **(e)** PC1 and **(f)** PC2; fluorescence loadings for **(g)** PC1 and **(h)** PC2 and **(i)** dominant processes influencing DIC identified using PC1 loadings: ocean dynamics (DYN), biological uptake of DIC (BIO) and others (NO).

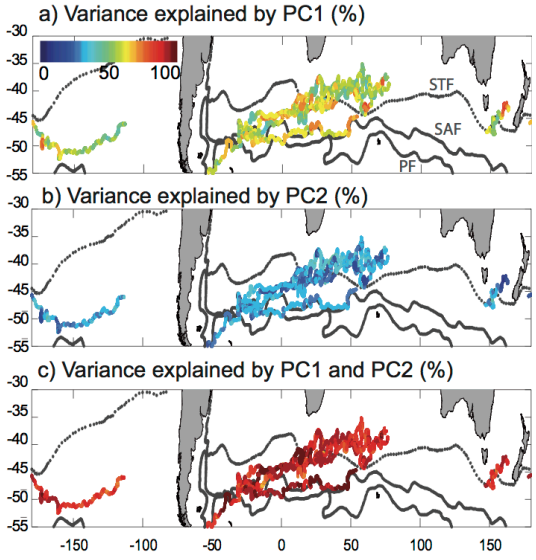

Fig. 5. Variance explained by **(a)** the first principal component (PC1), **(b)** the second principal component (PC2); **(c)** the cumulated variance explained by PC1 and PC2 obtained with the local PCA for DIC, SST and fluorescence.

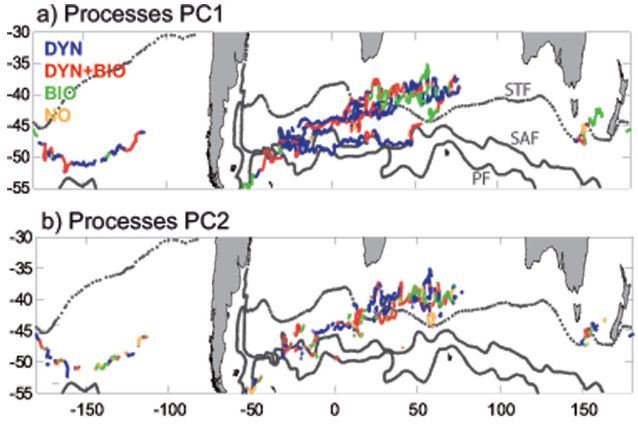

Fig. 6. Dominant processes influencing the variability at small spatial scales identified using **(a)** the first principal component (PC1), **(b)** the second principal component (PC2) loadings obtained with the local PCA for DIC, SST and fluorescence. Processes are ocean dynamical advection (DYN), biological uptake of DIC (BIO). NO indicates when none of these processes could be identified.

concentrations in the southern Pacific (Boutin and Merlivat, 2009). They found that the drifter 03740 crossed patches

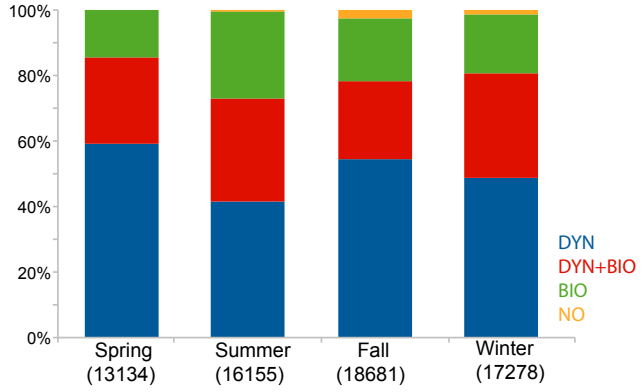

Fig. 7. The proportion of dominant processes identified for each season (in %). Note that there is a sampling bias toward winter and fall, spring being less sampled (the number of observations is indicated in parenthesis).

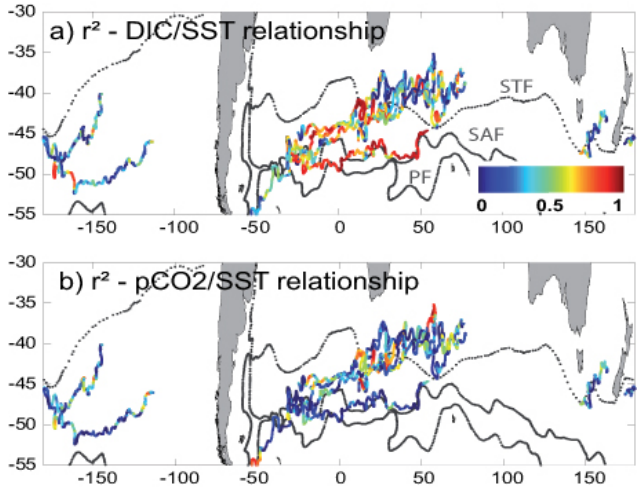

Fig. 8. Correlation coefficient (r^2) for the linear correlation between **(a)** SST and DIC; **(b)** SST and pCO_2. Fronts are indicated in grey.

of higher primary production between 142° W and 134° W, hence confirming the contribution of biological production in this region (see Fig. 3 Barbero et al., 2011). They also pointed out that these patches of biological activity were located along the SAF, which was at that time located north of its climatological position. This supports the idea that the ocean dynamics enhanced by the presence of the front was a key player in setting DIC variability.

The dominant drivers identified from PC2 mostly correspond to the contribution of ocean dynamics (respective to biological activity) in regions where biological activity (respective to ocean dynamics) dominates PC1 (Fig. 6a, b). Note that segments where neither ocean circulation nor biological activity can explain variations of DIC, SST and fluorescence on PC1 and PC2 correspond either to areas where salinity plays a significant role or to areas where no strong signature could be identified (indicated in brown in Fig. 6a, b).

3.3 How can satellite SST constrain the estimate of DIC small-scale variability?

The predominance of ocean dynamics and the maintenance of opposed gradients of DIC and SST down to small spatial scales suggests that SST can be used as a proxy of DIC variability on scales of 100 km. In situ DIC and SST are strongly linearly correlated in particular in regions where ocean circulation was identified as the dominant mechanism (see Sect. 3.1.2, Figs. 8a and 6a, b). Note that by contrast, surface pCO_2 and SST are only poorly correlated (Fig. 8b). Maps of DIC were reconstructed using the linear relationship derived locally between in situ SST and DIC and AMSR-E SST maps.

The method is illustrated in the case study area (Fig. 9). In autumn 2007, the drifter 13 060 followed the SAF, highlighted by the presence of a sharp satellite SST gradient and a dynamical boundary indicated by altimetry (black contours on Fig. 9). Between 18 March and 7 April, the drifter trajectory was wrapped around two mesoscale eddies (denoted E1 and E2), allowing the drifter to sample northern, warm DIC-poor waters trapped in E1 and southern, cold DIC-rich waters trapped in E2 (Fig. 9a, c and d). In this 20-day window centered on 28 March, in situ $\widehat{\text{DIC}}$ and $\widehat{\text{SST}}$ are strongly anticorrelated ($\widehat{\text{DIC}} = -9.69 \cdot \widehat{\text{SST}} + 0.09$, with $r^2 > 0.86$). In addition, the SST sampled by the drifter and the SST observed by the satellite AMSR interpolated in space and time at the drifter location are in good agreement (Fig. 9a and b). This gives us confidence that the map of $\widehat{\text{DIC}}_{\text{sat}}$ reconstructed from satellite SST and the local linear correlation obtained between $\widehat{\text{DIC}}$ and $\widehat{\text{SST}}$ provides a good estimate of the DIC variability at a small spatial scale (Fig. 9d). In the box covered by the drifter (45 to 49° E; 48 to 45 ° S), the reconstructed $\widehat{\text{DIC}}_{\text{sat}}$ varies between roughly −15 and 20 µmol kg^{-1}. SV100km$_{\text{sat}}$, estimated in 100 km × 100 km boxes along the drifter trajectory, has an average value of 10 µmol kg^{-1}, with higher values (up to 15 µmol kg^{-1}) in the vicinity of SAF and lower values (down to 5 µmol kg^{-1}) further from the SAF. This estimate of the variability of DIC, which relies on the instantaneous spatial distribution of SST and a linear correlation between DIC and SST, is relatively independent from the variability estimated using the high-pass filtered time series sampled by the drifters, the only link between the two being the linear correlation based on the time series. This second estimate given by SV100km$_{\text{sat}}$ (5 to 15 µmol kg^{-1}) is very similar to the SV100km estimated from the time series in this area (5 to 12 µmol kg^{-1} in Fig. 2j).

To strengthen the results obtained with the SV100km derived from time series, this second estimate is computed using all SST satellite images collocated with drifters trajectories available when the correlation coefficient, r^2, exceeds 0.7 (Fig. 3c). This estimate confirms the order of

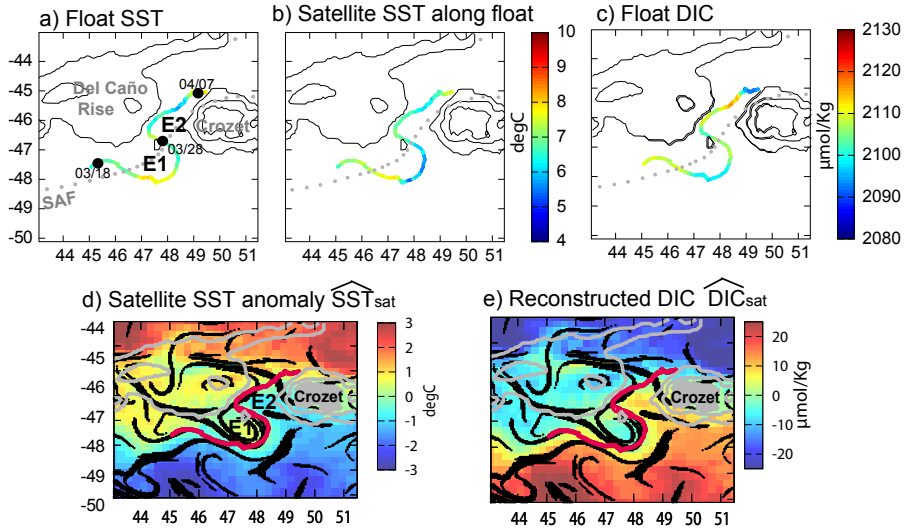

Fig. 9. Case study: **(a)** SST measured by drifter 13 060 between 18 March and 7 April 2007; **(b)** satellite AMSR SST collocated in time and space with the drifter; **(c)** DIC measured by drifter 13 060; **(d)** SST anomaly from satellite AMSR $\widehat{SST}_{sat}$ on 28 March 2007 and **(e)** $\widehat{DIC}_{sat}$ on 28 March 2007 reconstructed from $\widehat{SST}_{sat}$ and a DIC–SST linear relationship derived from drifter measurements ($\widehat{DIC} = -9.69 \cdot \widehat{SST} + 0.09$, with $r^2 > 0.86$). Dynamical boundaries derived from altimetry, i.e., unstable manifolds, are indicated in black (d'Ovidio et al., 2004). The drifter trajectory (in red) is wrapped around two eddies, denoted E1 and E2. Grey contours indicate the bathymetry.

magnitude of DIC variability at small spatial scales obtained from the time series (Fig. 3b), with typical gradients of 2–10 µmol k^{-1}, increasing to 10–15 µmol kg^{-1} in frontal areas and up to 15–30 µmol kg^{-1} in regions of high eddy kinetic energy or where biological activity was identified as a driving mechanism of DIC variability (Figs. 3b, c and 6a).

3.4 Does small-scale variability matter compared to large-scale and seasonal variability?

The variability of DIC identified at small spatial scales can be compared to the variability at larger spatial and temporal scales. Large-scale regional and latitudinal contrasts highlighted by the Glodap database primarily arise from the thermal effect on CO_2 solubility, the Revelle factor and the large-scale circulation (Fig. 1e, Williams and Follows, 2011). DIC temporal variability is dominated by the seasonality arising from the deepening of the mixed layer (ML) in winter and the biological uptake of DIC in summer. The extensive data set presented here captures the variability introduced by these various spatial and temporal scales (colored lines on Fig. 10). In the previous sections, the variability arising from small-scale structures was identified by filtering out temporal scales longer than 20 days and spatial scales larger than 500–1000 km (see Sect. 3.1.2). It is, however, relatively difficult to disentangle seasonal variations from large-scale regional variations along the drifters trajectories.

To estimate the variability introduced by large-scale regional contrasts in drifters' measurements, we used the Glodap annual value interpolated along the drifter trajectory (light grey on Fig. 10). Interestingly, these time series reconstructed from the interpolation of Glodap DIC at the drifter location reproduce a large part of the variations captured by the drifters, suggesting that large-scale regional contrasts account for a large part of the low-frequency variability sampled by the drifters (Fig. 10). In particular, we note that the large-scale gradients are well resolved by Glodap along drifters trajectories in the Atlantic and Indian sectors, where more observations are available (Fig. 10a–d and i). From this reconstructed time series we estimate large-scale regional gradients to be of the order of $\sim$ 50 to 100 µmol kg^{-1} over spatial scales of $\sim$ 5000–10 000 km (i.e., temporal scales of $\sim$ 6 months along the drifter trajectories), which is much smaller than the variability estimated at a small scale in this study (2–30 µmol kg^{-1} over 100 km).

To date, no climatology describes the seasonal cycle of DIC. To reconstruct the seasonal cycle of surface DIC, we used the 3-D Glodap annual values and a monthly climatology of mixed layer depth derived from Argo drifters (Sallée et al., 2010) (Fig. 11a and b). As in Mahadevan et al. (2011), the seasonality is estimated by averaging the Glodap values within the mixed layer. In winter, the ML deepens and surface DIC concentrations increase when averaged with high-DIC subsurface concentrations. In summer, restratification leads to lower estimates of surface DIC concentrations due to lower mixing with subsurface waters, hence mimicking the biological uptake of DIC. Two estimates of the seasonal cycles are obtained: the first one uses the mean value of the mixed layer depth in the $1° \times 1°$ box around the drifter sample (black lines on Fig. 10), whereas the second uses the maximum value of the mixed layer in that same box (dark grey lines on Fig. 10). The comparison between the two gives

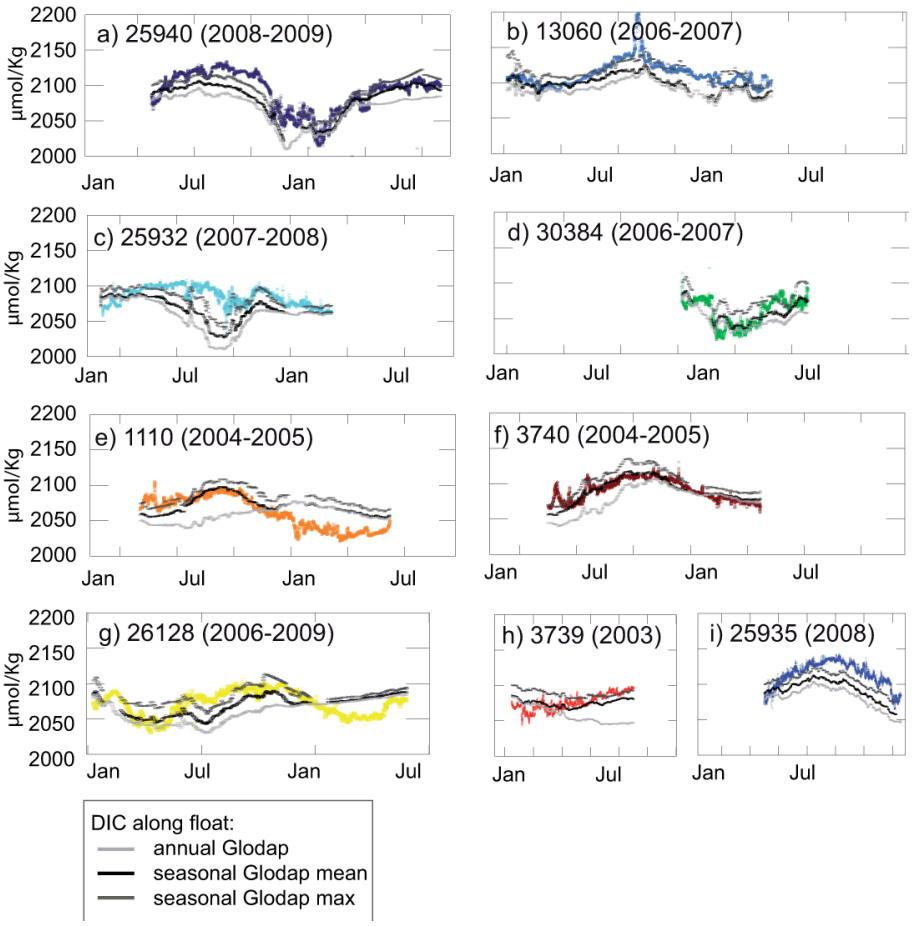

Fig. 10. DIC along CARIOCA drifters trajectories; DIC deduced from the pCO_2 sampled by the drifters (colored lines) is compared to the "annual Glodap DIC" and two estimates of the "seasonal Glodap DIC" along the drifters location. The "annual Glodap DIC" (light grey) shows the large-scale gradients of surface DIC in Glodap in a 5° by 5° box centered on the drifter location. The two "seasonal Glodap DIC" estimates were computed by averaging the vertical profile of Glodap DIC over monthly mixed layer depths. The "seasonal Glodap DIC mean" and "seasonal Glodap DIC max", respectively, correspond to the mean and maximum values obtained in each 5° by 5° box centered on the drifters trajectories (see Sect. 3.4), which gives an estimation of the seasonal signal on surface DIC concentrations.

an estimation of the method's sensitivity to interannual and small-scale variability of the ML. This reconstruction assumes that: (1) on an annual scale, summertime biological uptake of DIC is counterbalanced by wintertime physical input of DIC associated with the deepening of the ML; (2) the biological uptake of DIC is synchronous with the ML restratification and (3) Glodap values correspond to well-stratified, low-DIC summer conditions. We expect hypotheses 1 and 3 to be relatively valid in the Southern Ocean because of the predominant effect of winter mixing at high latitudes and because most of the profiles used to derive Glodap were sampled between October and April in this region (see Appendix Fig. A3). In contrast, hypothesis 2 may introduce lags in DIC seasonality.

The reconstructed seasonal DIC interpolated along the drifters trajectories captures most of the low-frequency signal observed in situ by the drifters (dark grey lines vs. colored lines on Fig. 10), which suggests that Glodap spatial variability and seasonal variability reconstructed from the ML climatology give a useful estimate of the regional patterns and seasonality of the DIC in the Southern Ocean. Note that part of the signal captured by the drifters, however, remains unexplained, most probably because of the interannual and small-scale variability, the assumptions made to compute the seasonal cycle (see 3 hypotheses above) and the biases introduced by undersampling in the ML climatology and the Glodap database. For example, the largest DIC differences (up to 25–50 µmol kg^{-1}) between drifters measurements and the reconstructed time series are observed in the Pacific sector and south of Tasmania (drifters 1110 and 3739) that are poorly sampled by Glodap (Fig. 10). When applied to the whole Southern Ocean, this estimate gives an amplitude of DIC seasonal variations (winter max – summer min) of the order of 10–50 µmol kg^{-1} (Fig. 11c). Our estimate is in agreement

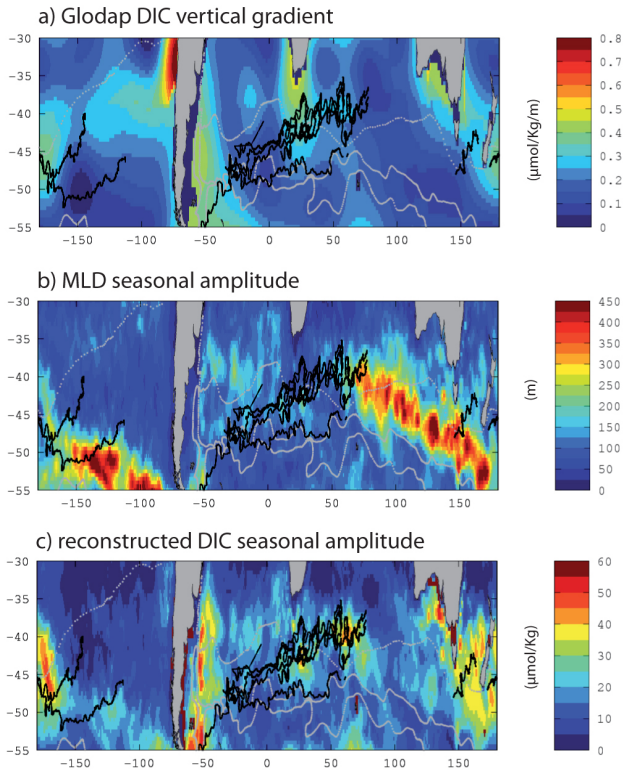

Fig. 11. (a) Vertical gradient of DIC between the surface and 200 m in Glodap database; **(b)** seasonal amplitude (annual max–annual min) of ML depth in the climatology derived from Argo drifters of Sallée et al. (2010); **(c)** DIC seasonal amplitude (annual max–annual min) reconstructed by averaging Glodap annual values over the ML monthly climatology. See text Sect. 3.4 for further details.

with the seasonality observed in the Indian sector during the Océan Indien Service d'Observation (OISO) cruises (60° E, 50–55° S), where it amounts to $\sim$10–30 µmol kg^{-1} (Metzl et al., 2006) and in the Pacific sector at the Munida time series south of New Zealand (171° E, 46° S), where it reaches 40 µmol kg^{-1} (Brix et al., 2013).

4 Discussion and conclusions

In this study, the pCO_2 and DIC variability at a small spatial scale in the Southern Ocean is estimated using an extensive data set of surface drifter measurements. Typical gradients on spatial scales of 100 km range from 5 to 50 µatm for pCO_2 and 2 to 30 µmol kg^{-1} for DIC. The result of DIC variability is supported by a second estimate based on SST satellite images and DIC–SST relationships at spatial scales of $\sim$100 km derived from drifters observations. Regions in which the CO_2 system has the highest variability mostly correspond to regions of high eddy kinetic energy or frontal zones. These estimates of the CO_2 system variability at a small scale are comparable to estimates obtained in the tropical Pacific (up to 30 µatm on scales of 50 km, Chen et al., 2007) northeast Atlantic (up to 25 µatm on scales of 25 km, Resplandy et al., 2009).

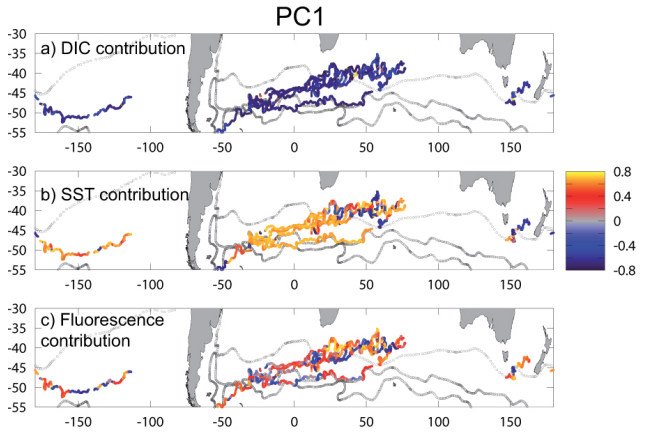

Fig. 12. PC1 loadings for DIC, SST and fluorescence. Note that principal component loadings are correlation coefficient between -1 and 1.

Using a principal component analysis, we found that the DIC variability at a small scale mostly arises from ocean dynamics. Although the circulation is identified as the first mechanism generating variability at small spatial scales, it results in relatively low variability with typical gradients of $\sim$2–10 µmol kg^{-1} over scales of 100 km, reaching values up to 10–15 µmol kg^{-1} in regions of fronts and high eddy kinetic energy. By contrast, when biological activity is identified as a key process in DIC distribution at small spatial scale, gradients are enhanced (with values up to 10–30 µmol kg^{-1} over scales of 100 km). This is in agreement with previous in situ observations that highlighted the higher spatial variability of biogeochemical parameters when primary productivity is enhanced (Metzl et al., 2006; Rangama et al., 2005).

It should be noted that the dominance of dynamical and biological processes inferred from this analysis could be biased in two ways. First, drifters tend to be concentrated along frontal jets, where the dynamical advection is particularly intense. This could exaggerate the contribution of dynamical advection, in particular in the Atlantic sector between the Polar and Subtropical Fronts (Fig 6). Second, DIC is calculated from alkalinity based on the approach of Lee et al. (2006), which itself integrates the large-scale salinity and temperature gradients. This method, when adapted to studies at the regional scale, does not account for the biologically driven changes in alkalinity that could occur on small spatial scales, such as in a productive eddy. Biologically driven changes in alkalinity are largely associated with the uptake of CO_3^{2-} when calcite is formed, the impact of other nutrients (nitrate, phosphate, silicate etc.) being negligible. We expect this bias to be relatively small in most regions sampled by the drifters, the production of calcite being very low in the region sampled by the drifters except north of 45° S (see Sarmiento

and Gruber, 2006, chap 9). Hence, this approximation could impact the results in the subtropical Indian sector, where the formation of calcite could represent ∼10% of the biological uptake of carbon. This could lead to an underestimation of DIC variations of ∼10% in small-scale structures where calcite is formed. However, we do not expect this bias to change the main result of the present study, which already identifies the subtropical Indian sector as the region with the highest biological contribution (Fig 6).

Modeling studies showed that both horizontal and vertical advection associated with small-scale structures can affect the distribution of DIC at small spatial scales and hence the surface pCO_2 (Mahadevan et al., 2004; Resplandy et al., 2009). Horizontally, the ocean circulation advects large-scale gradients down to small spatial scales. It is now widely accepted that mesoscale eddies, which dominate the variability at scales of the order of 100 km, horizontally transport and stir tracers such as DIC and temperature, resulting in a cascade of tracer variance to smaller scales (Abraham et al., 2000; Lévy and Klein, 2004). In addition, density gradients associated with small-scale features are associated with large vertical velocities (Capet et al., 2008; Lévy et al., 2012), that could transport deeper waters with high DIC concentration to the surface. It is generally very difficult to assess the contribution of vertical advection purely from observations. More specifically, the data set used here does not allow one to discriminate between the contributions of horizontal and vertical advection. First, large-scale horizontal and vertical gradients in the Southern Ocean are associated with a similar signature of increasing DIC concentration with decreasing temperature that can not be separated with the principal component analysis. In addition, our observations only describe surface waters and provide no information on vertical gradients. Nevertheless, the fact that dynamical advection alone results in relatively low variability in DIC except in zones of strong horizontal gradients (frontal zones) strongly suggests that the horizontal component of advection plays a major role in determining the variability at small spatial scales. The impact of episodic vertical mixing events (such as eddies or storms) on surface pCO_2 has been estimated in Mahadevan et al. (2011) using global monthly climatological data sets. They found that vertical mixing events could induce changes in DIC through the vertical input of DIC-rich subsurface waters and the enhancement of biological uptake. In agreement with previous studies based on observations (Chen et al., 2007) and models (Mahadevan et al., 2004; Resplandy et al., 2009), they found a relatively low impact on pCO_2 ($< 5\,\%$) due to compensations between biological uptake, DIC input and thermal effects.

This study confirms that seasonal variations are the dominant mode of variability of the CO_2 system in the Southern Ocean (Lenton et al., 2006). However, we find that small spatial-scale structures are a non-negligible source of variability for DIC, with amplitudes of about a third of the variations associated with the seasonality (2–30 µmol kg^{-1} vs. 10–50 µmol kg^{-1}). In addition, the amplitude of this variability is at least of the same order of magnitude as large-scale gradients and can be up to ∼ 10 times larger in regions of high eddy kinetic energy and biological activity. These small-scale processes are not captured by onboard observations and climate models used to derive carbon budgets. This issue must be considered in combination with the fact that seasonal cycles of pCO_2 and DIC in the Southern Ocean are still poorly described due to the lack of shipboard observations mainly during winter (Metzl et al., 2006). This has strong implication for our understanding of the carbon budget derived from observations (Barbero et al., 2011) but also from model simulations (Lenton et al., 2013), whose evaluations rely on these observations. Direct measurements being scarce, an alternative is to derive DIC from observed pCO_2, temperature and salinity fields. Although numerous observations of surface pCO_2 are available (Takahashi et al., 2009; Pfeil et al., 2012), the amount of DIC observations that can be derived is drastically lower. In Lenton et al. (2012), 75 000 surface DIC estimates could be computed from the 4.4 million individual measurements of the global database of Takahashi et al. (2009) after removing non-collocated measurements of pCO_2, SST and SSS and coastal data. Among these data, only few are located in the Southern Ocean, thus limiting the assessment of the seasonal cycle and small-scale variability of DIC.

In this work, the seasonal cycle of surface DIC is reconstructed from the annual Glodap data set and a mixed-layer climatology. This methodology has been previously used in Mahadevan et al. (2011) at global scale but was not validated. Here, we provide a validation of this method in the Southern Ocean using the months- to year-long high-frequency time series of the nine drifters deployed in the area. The fair agreement between in situ observations and the reconstructed seasonal DIC suggests that this method gives first-order estimates of the seasonal amplitude of surface DIC in the Southern Ocean that could be used for model evaluation. However, it should be kept in mind that the ability of this method is lower in poorly sampled regions, such as the Pacific sector, and that it provides stronger constraint on the timing of wintertime DIC enrichment than on the timing of summertime DIC consumption. Despite the limitations of the method, our findings provide a first step towards better understanding the contribution and amplitude of variability introduced by small-scale structures versus the variability introduced by large-scale contrasts, seasonality and interannual to decadal variability. This study suggests that care should be taken when inferring temporal changes (seasonality, interannual variability, decadal trends) from sparse observations. Indeed, these observations and the methods used do not take into account the variability on small spatial scales, while our results highlight the fact that the various spatial and temporal sources of variability can be of the same order of magnitude in some regions of the Southern Ocean.

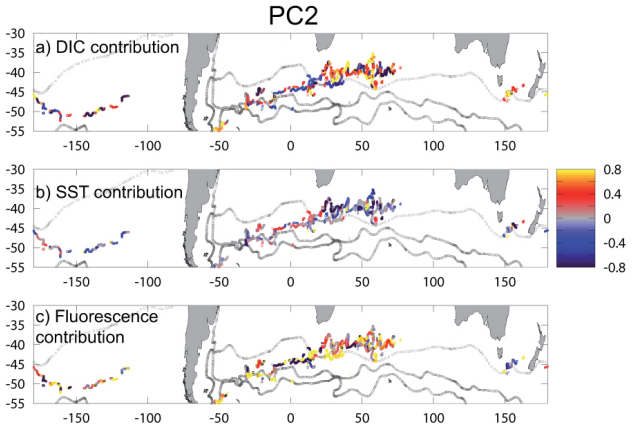

Fig. A1. PC2 loadings for DIC, SST and fluorescence. Note that principal component loadings are correlation coefficients between −1 and 1.

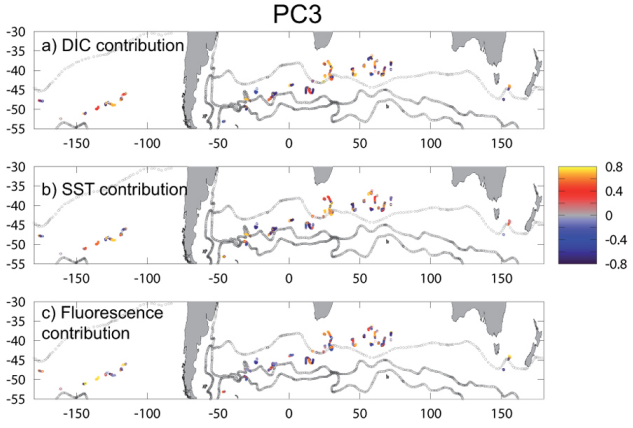

Fig. A2. PC3 loadings for DIC, SST and fluorescence. Note that principal component loadings are correlation coefficients between −1 and 1.

Appendix A

Principal Component Analysis loadings of PC1, PC2 and PC3 obtained with DIC, SST and fluorescence (Figs. 12–A2). The loadings are shown only when the PC relates strongly to the variations of DIC and when it explains a significant part of the variance at a small scale (i.e., when the carbon variable loading on this PC is ≥ 0.3 and the explained variance of this PC is $\geq 20\,\%$, see Sect. 2.3).

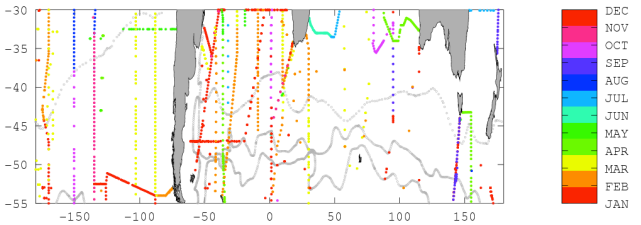

Fig. A3. Distribution and sampling month of DIC used to derive the 3-D-gridded Glodap product in the Southern Ocean.

Acknowledgements. Support was provided by the European Integrated project CARBOOCEAN and EU FP7 project CARBOCHANGE: Changes in carbon uptake and emissions by oceans in a changing climate, which received funding from the European Commission's Seventh Framework Programme under grant agreement no. 264879. We thank L. Beaumont and T. Danguy from technical division of Institut National des Sciences de l'Univers for supervising CARIOCA assembly and performing thorough CARIOCA calibrations. We sincerely thank Francesco d'Ovidio for providing and maintaining the LAgrangian Manifolds and Trajectories Analyser (LAMTA) toolbox. Altimeter products were produced by Ssalto/Duacs and distributed by AVISO with support from the Centre National d'Études Spatiales.

Edited by: V. Brovkin

The publication of this article is financed by CNRS-INSU.

References

Abraham, E. R., Law, C. S., Boyd, P. W., Lavender, S. J., Maldonado, M. T., and Bowie, A. R.: Importance of stirring in the development of an iron-fertilized phytoplankton bloom, Nature, 407, 727–730, doi:10.1038/35037555, 2000.

Barbero, L., Boutin, J., Merlivat, L., Martin, N., Takahashi, T., Sutherland, S. C., and Wanninkhof, R.: Importance of water mass formation regions for the air?sea CO_2 flux estimate in the Southern Ocean, Global Biogeochem. Cy., 25, GB1005, doi:10.1029/2010GB003818, 2011.

Boutin, J. and Merlivat, L.: New in situ estimates of carbon biological production rates in the Southern Ocean from CARIOCA drifter measurements, Geophys. Res. Lett., 36, L13608, doi:10.1029/2009GL038307, 2009.

Boutin, J., Merlivat, L., Hénocq, C., Martin, N., and Sallée, J. B.: Air-sea CO_2 flux variability in frontal regions of the Southern Ocean from CARIOCA drifters, Limnol. Oceanogr., 53, 2062–2079, 2008.

Brix, H., Currie, K. I., and Mikaloff Fletcher, S. E.: Seasonal variability of the carbon cycle in subantarctic surface water in the South West Pacific, Global Biogeochem. Cy., 27, 200–211, doi:10.1002/gbc.20023, 2013.

Capet, X., Colas, F., Penven, P., Marchesiello, P., and McWilliams, J. C.: Eastern boundary subtropical upwelling systems, in: Eddy Resolving Ocean Modeling, edited by: Hecht, M. W. and Hasumi, H., Geoph. Monog. Series, Washington DC, 117, 131–147, 2008.

Chen, F., Cai, W.-J., Benitez-Nelson, C., and Wang, Y.: Sea surface "pco_2-sst" relationships across a cold-core cyclonic eddy: implications for understanding regional variability and air–sea gas exchange, Geophys. Res. Lett., 34, L10603, doi:10.1029/2006GL028058, 2007.

Copin-Montégut, C., Begovic, M., and Merlivat, L.: Variability of the partial pressure of CO_2 on diel to annual time scales in the northwestern Mediterranean Sea, Sci. Mar., 85, 169–189, doi:10.1016/j.marchem.2003.10.005, 2004.

Dandonneau, Y.: Sea-surface partial pressure of carbon dioxide in the eastern equatorial Pacific (August 1991 to October 1992): a multivariate analysis of physical and biological factors, Deep-Sea Res. Pt. II, 42, 349–364, doi:10.1016/0967-0645(95)00017-K, 1995.

d'Ovidio, F., Fernández, V., Hernández-García, E., and López, C.: Mixing structures in the Mediterranean Sea from finite-size Lyapunov exponents, Geophys. Res. Lett., 31, L17203, doi:10.1029/2004GL020328, 2004.

Gruber, N., Gloor, M., Fletcher, S. E. M., Doney, S. C., Dutkiewicz, S., Follows, M. J., Gerber, M., Jacobson, A. R., Joos, F., Lindsay, K., Menemenlis, D., Mouchet, A., Müller, S. A., Sarmiento, J. L., and Takahashi, T.: Oceanic sources, sinks, and transport of atmospheric CO_2, Global Biogeochem. Cy., 23, GB1005, doi:10.1029/2008GB003349, 2009.

Ito, T., Marshall, J., and Follows, M.: What controls the uptake of transient tracers in the Southern Ocean?, Global Biogeochem. Cy., 18, GB2021, doi:10.1029/2003GB002103, 2004.

Key, R. M., Kozyr, A., Sabine, C. L., Lee, K., Wanninkhof, R., Bullister, J. L., Feely, R. A., Millero, F. J., Mordy, C., and Peng, T.-H.: A global ocean carbon climatology: results from Global Data Analysis Project (GLODAP), Global Biogeochem. Cy., 18, GB4031, doi:10.1029/2004GB002247, 2004.

Lee, K., Tong, L. T., Millero, F. J., Sabine, C. L., Dickson, A. G., Goyet, C., Park, G.-H., Wanninkhof, R., Feely, R. A., and Key, R. M.: Global relationships of total alkalinity with salinity and temperature in surface waters of the world's oceans, Geophys. Res. Lett., 33, L19605, doi:10.1029/2006GL027207, 2006.

Lehahn, Y., d'Ovidio, F., Lévy, M., and Heitzel, E.: Stirring of the Northeast Atlantic spring bloom: a lagrangian analysis based on multi-satellite data, J. Geophys. Res., 112, C08005, doi:10.1029/2006JC003927, 2007.

Lenton, A., Matear, R. J., and Tilbrook, B.: Design of an observational strategy for quantifying the Southern Ocean uptake of CO_2, Global Biogeochem. Cy., 20, GB4010, doi:10.1029/2005GB002620, 2006.

Lenton, A., Metzl, N., Takahashi, T., Kuchinke, M., Matear, R. J., Roy, T., Sutherland, S. C., Sweeney, C., and Tilbrook, B.: The observed evolution of oceanic pCO_2 and its drivers over the last two decades, Global Biogeochem. Cy., 26, GB2021, doi:10.1029/2011GB004095, 2012.

Lenton, A., Tilbrook, B., Law, R. M., Bakker, D., Doney, S. C., Gruber, N., Ishii, M., Hoppema, M., Lovenduski, N. S., Matear, R. J., McNeil, B. I., Metzl, N., Mikaloff Fletcher, S. E., Monteiro, P. M. S., Rödenbeck, C., Sweeney, C., and Takahashi, T.: Sea-air CO_2 fluxes in the Southern Ocean for the period 1990–2009, Biogeosciences, 10, 4037–4054, doi:10.5194/bg-10-4037-2013, 2013.

Lévy, M. and Klein, P.: Does the low frequency variability of mesoscale dynamics explain a part of the phytoplankton and zooplankton spectral variability?, P. R. Soc. London, 460, 1673–1683, doi:10.1098/rspa.2003.1219, 2004.

Lévy, M., Ferrari, R., Franks, P., Martin, A., and Rivire, P.: Bringing physics to life at the submesoscale, Geophys. Res. Lett., 39, L14602, doi:10.1029/2012GL052756, 2012.

Lohrenz, S. E., Cai, W., Chen, F., Chen, X., and Tuel, M.: Seasonal variability in air-sea fluxes of CO_2 in a river influenced coastal margin, J. Geophys. Res., 115, C10034, doi:10.1029/2009JC005608, 2009.

Lovenduski, N. S., Gruber, N., and Doney, S. C.: Toward a mechanistic understanding of the decadal trends in the Southern Ocean carbon sink, Global Biogeochem. Cy., 22, GB3016, doi:10.1029/2007GB003139, 2008.

Mahadevan, A., Lévy, M., and Mémery, L.: Mesoscale variability of sea surface pCO_2: What does it respond to?, Global Biogeochem. Cy., 18, GB1017, doi:10.1029/2003GB002102, 2004.

Mahadevan, A., Tagliabue, A., Bopp, L., Lenton, A., Mémery, L., and Lévy, M.: Impact of episodic vertical fluxes on sea surface pco_2, Philos. T. R. Soc. A, 369, 2009–2025, doi:10.1098/rsta.2010.0340, 2011.

McNeil, B. I., Metzl, N., Key, R. M., Matear, R. J., and Corbiere, A.: An empirical estimate of the southern ocean air-sea CO_2 flux, Global Biogeochem. Cy., 21, GB3011, doi:10.1029/2007GB002991, 2007.

Metzl, N.: Decadal increase of oceanic carbon dioxide in Southern Indian Ocean surface waters (1991–2007), Deep-Sea Res. Pt. II, 56, 607–619, doi:10.1016/j.dsr2.2008.12.007, 2009.

Metzl, N., Brunet, C., Jabaud-Jan, A., Poisson, A., and Schauer, B.: Summer and winter air-sea $\{CO_2\}$ fluxes in the Southern Ocean, Deep-Sea Res. Pt I, 53, 1548–1563, doi:10.1016/j.dsr.2006.07.006, 2006.

Mikaloff Fletcher, S. E., Gruber, N., Jacobson, A. R., Gloor, M., Doney, S. C., Dutkiewicz, S., Gerber, M., Follows, M., Joos, F., Lindsay, K., Menemenlis, D., Mouchet, A., Müller, S. A., and Sarmiento, J. L.: Inverse estimates of anthropogenic CO_2 uptake, transport, and storage by the ocean, Global Biogeochem. Cy., 20, GB2002, doi:10.1029/2005GB002530, 2006.

Murata, A.: Increased surface seawater pCO_2 in the eastern Bering Sea shelf: an effect of blooms of *coccolithophorid Emiliania huxleyi*?, Global Biogeochem. Cy., 20, GB4006, doi:10.1029/2005GB002615, 2006.

Orr, J. C., Maier-Reimer, E., Mikolajewicz, U., Monfray, P., Sarmiento, J. L., Toggweiler, J. R., Taylor, N. K., Palmer, J., Gruber, N., Sabine, C. L., Le Quéré, C., Key, R. M., and Boutin, J.: Estimates of anthropogenic carbon uptake from four three-dimensional global ocean models, Global Biogeochem. Cy., 15, 43–60, doi:10.1029/2000GB001273, 2001.

Pfeil, B., Olsen, A., Bakker, D. C. E., Hankin, S., Koyuk, H., Kozyr, A., Malczyk, J., Manke, A., Metzl, N., Sabine, C. L., Akl, J., Alin, S. R., Bates, N., Bellerby, R. G. J., Borges, A., Boutin, J., Brown, P. J., Cai, W.-J., Chavez, F. P., Chen, A., Cosca, C., Fassbender, A. J., Feely, R. A., González-Dávila, M., Goyet, C., Hales, B., Hardman-Mountford, N., Heinze, C., Hood, M., Hoppema, M., Hunt, C. W., Hydes, D., Ishii, M., Jo-

hannessen, T., Jones, S. D., Key, R. M., Körtzinger, A., Landschützer, P., Lauvset, S. K., Lefèvre, N., Lenton, A., Lourantou, A., Merlivat, L., Midorikawa, T., Mintrop, L., Miyazaki, C., Murata, A., Nakadate, A., Nakano, Y., Nakaoka, S., Nojiri, Y., Omar, A. M., Padin, X. A., Park, G.-H., Paterson, K., Perez, F. F., Pierrot, D., Poisson, A., Ríos, A. F., Santana-Casiano, J. M., Salisbury, J., Sarma, V. V. S. S., Schlitzer, R., Schneider, B., Schuster, U., Sieger, R., Skjelvan, I., Steinhoff, T., Suzuki, T., Takahashi, T., Tedesco, K., Telszewski, M., Thomas, H., Tilbrook, B., Tjiputra, J., Vandemark, D., Veness, T., Wanninkhof, R., Watson, A. J., Weiss, R., Wong, C. S., and Yoshikawa-Inoue, H.: A uniform, quality controlled Surface Ocean CO_2 Atlas (SOCAT), Earth Syst. Sci. Data, 5, 125–143, doi:10.5194/essd-5-125-2013, 2013.

Pollard, T., R., Venables, H. J., Read, J. F., and Allen, J. T.: Large-scale circulation around the Crozet Plateau controls an annual phytoplankton bloom in the Crozet Basin, Deep-Sea Res. Pt. II, 54, 1915–1929, doi:10.1016/j.dsr2.2007.06.012, 2007.

Rangama, Y., Boutin, J., Etcheto, J., Merlivat, L., Takahashi, T., Delille, B., Frankignoulle, M., and Bakker, D. C. E.: Variability of the net air-sea CO_2 flux inferred from shipboard and satellite measurements in the Southern Ocean south of Tasmania and New Zealand, J. Geophys. Res., 110, C09005, doi:10.1029/2004JC002619, 2005.

Read, J., Pollard, R., and Allen, J.: Sub-mesoscale structure and the development of an eddy in the subantarctic front north of the Crozet Islands, Deep-Sea Res. Pt. II, 54, 1930–1948, doi:10.1016/j.dsr2.2007.06.013, 2007.

Resplandy, L., Lévy, M., d'Ovidio, F., and Merlivat, L.: Impact of submesoscale variability in estimating the air-sea CO_2 exchange: results from a model study of the POMME experiment, Global Biogeochem. Cy., 23, GB1017, doi:10.1029/2008GB003239, 2009.

Rintoul, S. R., Hughes, C., and Olbers, D.: The Antarctic circumpolar current system, in: Ocean Circulation and Climate, edited by: Sieddler, G., Church, J., and Gould, J., Academic Press, London, 271–302, 2001.

Sallée, B. J., Speer, K., and Rintoul, S. R.: Zonnally asymmetric response of the Southern Ocean mixed-layer depth to the Southern Annular Mode, Nat. Geosci., 3, 273–279, 2010.

Sarmiento, J. L. and Gruber N.: Ocean Biogeochemical Dynamics, Princeton, Woodstock, Princeton University Press, 528 pp., 2006.

Séférian, R., Bopp, L., Swingedouw, D., and Servonnat, J.: Dynamical and biogeochemical control on the decadal variability of ocean carbon fluxes, Earth Syst. Dynam., 4, 109–127, doi:10.5194/esd-4-109-2013, 2013.

Takahashia, T., Sutherland, S. C., Wanninkhof, R., Sweeney, C., Feely, R. A., Chipman, D. W., Hales, B., Friederich, G., Chavez, F., Sabine, C., Watson, A., Bakker, D. C. E., Schuster, U., Metzl, N., Yoshikawa-Inoue, H., Ishii, M., Midorikawa, T., Nojiri, Y., Kórtzinger, A., Steinhoff, T., Hoppema, M., Olafsson, J., Arnarson, T. S., Tilbrook, B., Johannessen, T., Olsen, A., Bellerby, R., Wong, C. S., Delille, B., Bates, N. R., and de Baar, H. J. W.: Climatological mean and decadal change in surface ocean pCO_2, and net sea-air CO_2 flux over the global oceans, Deep-Sea Res-Pt. II, 56, 554–577, doi:10.1016/j.dsr2.2008.12.009, 2009.

Tortell, P. D., Guéguen, C., Long, M. C., Payne, C. D., Lee, P., and DiTullio, G. R.: Spatial variability and temporal dynamics of surface water pCO_2, O_2/Ar and dimethylsulfide in the Ross Sea, Antarctica, Deep-Sea Res. Pt. I, 58, 241–259, doi:10.1016/j.dsr.2010.12.006, 2011.

Venables, H. J., Pollard, T. R., and Popova, E. E.: Physical conditions controlling the development of a regular phytoplankton bloom north of the Crozet Plateau, Southern Ocean, Deep-Sea Res. Pt. II, 54, 1949–1965, doi:10.1016/j.dsr2.2007.06.014, 2007.

Williams, R. G. and Follows, M. J.: Ocean Dynamics and the Carbon Cycle, Cambridge University Press, 2011.